Published in final edited form as:
J Control Release. 2011 May 30; 152(1): 37–48. doi:10.1016/j.jconrel.2011.01.009.

Tuning Core *vs.* Shell Dimensions to Adjust the Performance of Nanoscopic Containers for the Loading and Release of Doxorubicin

Lily Yun Lin[a,b], **Nam S. Lee**[a,b], **Jiahua Zhu**[c], **Andreas M. Nyström**[d], **Darrin J. Pochan**[c], **Richard B. Dorshow**[e], and **Karen L. Wooley**[a,*]

Lily Yun Lin: yun.lin@chem.tamu.edu; Nam S. Lee: nam.lee@chem.tamu.edu; Jiahua Zhu: jhzhu@udel.edu; Andreas M. Nyström: andreas.nystrom@ki.se; Darrin J. Pochan: pochan@udel.edu; Richard B. Dorshow: richard.dorshow@covidien.com; Karen L. Wooley: wooley@chem.tamu.edu

[a] Departments of Chemistry and Chemical Engineering, Texas A&M University, College Station, TX 77842-3012

[b] Department of Chemistry, Washington University in St. Louis, Saint Louis, MO 63130-4899

[c] Department of Materials Science and Engineering, University of Delaware, Newark, DE 19716-3106

[d] Department of Neuroscience and The Swedish Medical Nanoscience Center, Karolinska Institutet, SE-17177 Stockholm, Sweden

[e] Covidien Pharmaceuticals R&D, Hazelwood, MO 63042

Abstract

Detailed studies were performed to probe the effects of the core and shell dimensions of amphiphilic, shell crosslinked, knedel-like polymer nanoparticles (SCKs) on the loading and release of doxorubicin (DOX), a widely-used chemotherapy agent, in aqueous buffer, as a function of the solution pH. Effects of the nanoparticle composition were held constant, by employing SCKs constructed from a single type of amphiphilic diblock copolymer, poly(acrylic acid)-*b*-polystyrene (PAA-*b*-PS). A series of four SCK nanoparticle samples, ranging in number-average hydrodynamic diameter from 14–30 nm, was prepared from four block copolymers having different relative block lengths and absolute degrees of polymerization. The ratios of acrylic acid to styrene block lengths ranged from 0.65 to 3.0, giving SCKs with ratios of shell to core volumes ranging from 0.44 to 2.1. Although the shell thicknesses were calculated to be similar (1.5–3.1 nm by transmission electron microscopy (TEM) calculations and 3.5–4.9 nm by small angle neutron scattering (SANS) analyses), two of the SCK nanoparticles had relatively large core diameters (19 ± 2 and 20 ± 2 nm by TEM; 17.4 and 15.3 nm by SANS), while two had similar, smaller core diameters (11 ± 2 and 13 ± 2 nm by TEM; 9.0 and 8.9 nm by SANS). The SCKs were capable of being loaded with 1500–9700 DOX molecules per each particle, with larger numbers of DOX molecules packaged within the larger core SCKs. Their shell-to-core volume ratio showed impact on the rates and extents of release of DOX, with the volume occupied by the poly(acrylic acid) shell relative to the volume occupied by the polystyrene core correlating inversely with the

[*]wooley@chem.tamu.edu, Texas A&M University, Department of Chemistry, P.O. Box 30012, 3255 TAMU, College Station, TX 77842-3012, Tel. (979) 845-4077, Fax (979) 862-1137.

diffusion-based release of DOX. Given that the same amount of polymer was used to construct each SCK sample, SCKs having smaller cores and higher acrylic acid *vs*. styrene volume ratios were present at higher concentrations than were the larger core SCKs, and gave lower final extents of release., Higher final extents of release and faster rates of release were observed for all DOX-loaded particle samples at pH 5.0 *vs*. pH 7.4, respectively, *ca*. 60% *vs*. 40% at 60 h, suggesting promise for enhanced delivery within tumors and cells. By fitting the data to the Higuchi model, quantitative determination of the kinetics of release was made, giving rate constants ranging from 0.0431 to 0.0540 $h^{-½}$ at pH 7.4 and 0.106 to 0.136 $h^{-½}$ at pH 5.0. In comparison, the non-crosslinked polymer micelle analogs exhibited rate constants for release of DOX of 0.245 and 0.278 $h^{-½}$ at pH 7.4 and 5.0, respectively. These studies point to future directions to craft sophisticated devices for controlled drug release.

Keywords

core-shell nanoparticles; block copolymers; doxorubicin; drug delivery; nanoparticle dimensions; release kinetics

1. Introduction

Synthetic materials that are capable of sequestering, containing and releasing biologically-active agents have been of great interest for many years, as drugs and drug delivery systems. Inspiration for the designs of such materials comes from a variety of sources. For instance, the translation of polymeric ion-exchange resins into microparticles for, ideally, irreversible sequestration of bile acids or phosphates has led to the development of polymer drugs for lowering of serum cholesterol (*e.g.* WelChol®) or phosphate levels (*e.g.* Renagel®), respectively. Most often, however, synthetic materials are expected to retain their guests for a limited period of time and then allow for their release at controlled rates and under predetermined conditions. Such situations demand higher degrees of engineering complexity with respect to the synthetic material structure, composition, and morphology.

Nature has often provided the concepts and templates from which simple structures can be fabricated to provide sophisticated performances as hosts for packaging and releasing therapeutic guests [1]. As examples, viruses and lipoproteins are stealthy, naturally-occurring vehicles for targeted delivery of nucleic acids and cholesterol esters, respectively. Both viruses and lipoproteins feature architectural characteristics that would be favorable for a drug delivery system, such as: 1) nanoscopic dimensions to protect guest molecules having limited stability from their surroundings; 2) availability and accessibility of targeting moieties on the surface to achieve localized delivery; 3) robust and stealth structural integrity [2–4]. Although the synthetic and biological processes for tailoring of such natural vehicles have witnessed significant advance [5–12], synthetic materials provide unique opportunities, including versatility of structure and composition, facile engineering, variation of parameters, control of stability *vs*. degradability, and avoidance of potential immunological effects. Many of these synthetic systems are micro/nano scale particulates prepared from polymers that are self assembled into constructs that resemble the naturally-occurring vehicles. The evolution of modern synthetic polymer chemistry and techniques for self assembly have progressed from homogeneous macro- or microscopic materials to complex and well-defined multi-compartment nanostructured particles that retain structural integrity while allowing for tailored surface chemistry for advanced applications, such as tissue selective targeting [13].

Polymer micelles, assembled from amphiphilic block copolymers, which mimic biological entities have been investigated for a number of potential applications that take advantage of

their core-shell morphology and tunable surface chemistry [2, 14–19]. The core-shell architecture enables the polymer micelle to incorporate hydrophobic drugs into the core domain that serves as a non-aqueous reservoir *via* either physical entrapment or covalent linkages, thereby increasing the solubility and stability of the hydrophobic drugs under physiological conditions. The shell domain, in turn, can protect the drug from its surroundings, modulating the pharmacokinetics and disposition of the carrier, and allowing manipulation over the surface chemistry [20]. In contrast, micelles can only maintain their morphological integrities at concentrations above the critical micelle concentration (CMC) and are dynamic systems, potentially limiting their use as injectable drug carriers. Structural reorganization of the micellar structure will then result in dissociation of the therapeutic cargo and loss of sustained/controlled delivery. In addition, the polymeric assembly is subjected to change upon altering parameters in the surrounding environment, *e.g.*, ionic strength, pH, *etc*. [21–24]. Such factors have been used as a trigger for controlled release in specific tissue, such as in acidic tumor environments [25]. Block copolymer micellar assemblies have also taken advantage of hydrolytically-degradable polymer segments to mediate their controlled release performances, such as those derived from lactide and/or glycolide, for which a rich literature describes extensive study of their physical, chemical and biological properties in their utilization as platforms for drug packaging and release [26–33]. Most recently, Park and co-workers reported successful preparation of monodisperse microparticles arising from biodegradable poly(lactic-*co*-glycolic acid) through a top-down hydrogel template strategy--a unique nanofabrication method that allowed for control over the dimensions of these microparticles. Through release studies of various drug molecules, including progesterone, felodipine, risperidone and paclitaxel, the authors investigated the impact of size and shape on the drug release kinetics [34]. Probing the drug release effects of the particle dimensions on the nanoscale, may be accomplished through the synthesis of block copolymer precursors with different block lengths, thereby creating micelles with independently tuned core/shell sizes.

To overcome the limitations that the CMC of micelles poses on intravenous-type drug carriers [35–38], our research group and others have explored crosslinked micellar constructs, such as shell crosslinked knedel-like nanoparticles (SCKs), that combine the amphiphilic core-shell morphology of polymer micelles with stabilizing crosslinkers isolated throughout the peripheral shell layer [39]. Due to the regioselective crosslinks in the peripheral shell region, these nanoscale assemblies can be diluted without disassembly, and have increased dimensional stability compared to their non-crosslinked micellar counterparts [1, 40–42]. The core of the SCKs can retain its host capabilities, because the lack of crosslinks in the core region maintains chain mobility and access to the core volume, for sequestering of guests [43–45]. Moreover, just as in the case of macroscopic crosslinked networks originating from linear polymers [46], the readily adjustable shell crosslinking density allows for gating of the transport of those guests into and out of the core domain, while retaining the structural integrity of the SCK nanostructures [47]. With the distinctively different dimensions, compositions and structures of the core and shell domains of SCKs, and an ability to modify each independently, probing the effects of each is of great interest.

In our recent work, we have investigated the effects of the chemical composition and thermal characteristics of the hydrophobic core polymer material for the loading and release of doxorubicin (DOX) [48], a widely used chemotherapy drug for first line treatment of metastatic breast cancer, as well as other therapeutic regimes. The two classes of SCKs used in our previous study were constructed from poly(acrylic acid)-based (PAA) amphiphilic diblock copolymers with either glassy amorphous polystyrene (PS) block segment, possessing a high glass transition temperature (T_g), or semicrystalline poly(octadecyl acrylate-*co*-decyl acrylate) (P(ODA-*co*-DA)), possessing a low T_g and a crystalline melting temperature (T_m). The T_m of the P(ODA-*co*-DA) core domains could be tuned to be either

below or above physiological temperature [49]. It was demonstrated that the SCKs containing core material with higher T_g and T_m values retained DOX to higher loading extents and resulted in slower release rates. However, the release profiles were similar, which suggested that the release behavior of these two classes of SCKs was governed predominantly by the core-shell morphology of these nanoparticles and was less dependent upon the core composition [48]. In this current study, we probed effects of the core and shell dimensions, independently, on the loading and release of small molecule guests. Effects of composition were held constant, by employing SCKs constructed from a single type of amphiphilic diblock copolymer, poly(acrylic acid)-*b*-polystyrene (PAA-*b*-PS), and using DOX as a model chemotherapeutic compound.

2. Materials and methods

2.1. Materials

All chemicals were purchased from Aldrich Chemical Co. (St. Louis, MO) and used without further purification unless otherwise noted. Slide-A-Lyzer dialysis cassettes (10 kDa molecular weight cut-off, MWCO) were purchased from Pierce Biotech. (Rockford, IL). Amicon® ultra centrifugal filter devices (30 kDa MWCO) were purchased from Millipore Corp. (Bedford, MA). The Supor 25 mm 0.1 μm Spectra/Por Membrane tubes (MWCO 6–8 kDa), used for dialysis, were purchased from Spectrum Medical Industries Inc. Nanopure water (18 MΩ·cm) was acquired by means of a Milli-Q water filtration system, Millipore Corp. (Bedford, MA).

2.2. Instruments

^{1}H NMR and ^{13}C NMR spectra were collected on a Varian Mercury 300 spectrometer, using the residual solvent signal as internal standard. Infrared spectra were acquired on an IR Prestige 21 instrument from Shimadzu Corporation (Columbia, MD). UV-Vis spectra were collected at 37 °C in the region of 200 – 800 nm, using a Varian Cary 100 Bio UV-visible spectrophotometer. The molar extinction coefficient (ε) of doxorubicin (ε = 13050 $M^{-1}cm^{-1}$ at 488 nm) was determined by a calibration curve in DMFPBS, 4:1. The DOX concentrations in the nanoparticles were determined by UV-vis spectroscopy, measured directly in the aqueous DOX-nanoparticle solution aliquots as a function of time.

Gel permeation chromatography was performed on a Waters Chromatography, Inc., 1515 isocratic HPLC pump equipped with an inline degasser, a model PD2020 dual-angle, light scattering detector (Precision Detectors, Inc.), a model 2414 differential refractometer (Waters, Inc.), and four PL_{gel} polystyrene-*co*-divinylbenzene gel columns (Polymer Laboratories, Inc.) connected in series: 5 μm Guard (50 × 7.5 mm), 5 μm Mixed C (300 × 7.5 mm), 5 μm 10^4 (300 × 7.5 mm), and 5 μm 500 Å (300 × 7.5 mm) using the Breeze (version 3.30, Waters, Inc.) software. The instrument was operated at 35 °C with THF as eluent (flow rate set to 1.0 mL/min). Polymer solutions were prepared at a known concentration (*ca*. 3 mg/mL) and an injection volume of 200 μL was used. Data collection was performed with Precision Acquire 32 Acquisition program (Precision Detectors, Inc.) and analyses were carried out using Discovery32 software (Precision Detectors, Inc.) with a system calibration curve generated from plotting molecular weight as a function of retention time for a series of broad polydispersity poly(styrene) standards.

Glass transition temperatures (T_g) were measured by differential scanning calorimetry on a Mettler-Toledo DSC822® (Mettler-Toledo, Inc., Columbus, OH), with a heating rate of 10 °C/min. Measurements were analyzed using Mettler-Toledo Star^e v. 7.01 software. The T_g was taken as the midpoint of the inflection tangent, upon the third heating scan. Thermogravimetric analysis was performed under N_2 atmosphere using a Mettler-Toledo

model TGA/SDTA851[e], with a heating rate of 5 °C/min. Measurements were analyzed using Mettler-Toledo Star[e] v. 7.01 software.

Dynamic light scattering measurements were conducted with a Brookhaven Instruments, Co. (Holtsville, NY) DLS system equipped with a model BI-200SM goniometer, BI-9000AT digital correlator, and a model EMI-9865 photomultiplier, and a model Innova 300 Ar ion laser operated at 514.5 nm (Coherent Inc., Santa Clara, CA). Measurements were made at 25 ± 1 °C. Prior to analysis, solutions were filtered through a 0.45 μm Millex®-GV PVDF membrane filter (Millipore Corp., Medford, MA) to remove dust particles. Scattered light was collected at a fixed angle of 90°. The digital correlator was operated with 522 ratio spaced channels, and initial delay of 5 μs, a final delay of 50 ms, and a duration of 8 minutes. A photomultiplier aperture of 400 μm was used, and the incident laser intensity was adjusted to obtain a photon counting of between, 200 and 300 kcps. The calculations of the particle size distributions and distribution averages were performed with the ISDA software package (Brookhaven Instruments Company), which employed single-exponential fitting, Cumulants analysis, and CONTIN particle size distribution analysis routines. All determinations were average values from ten measurements.

Transmission electron microscopy (TEM) bright-field imaging was conducted on a Hitachi H-7500 microscope, operating at 80 kV. The samples were prepared as follows: 4 μL of the dilute solution (with a polymer concentration of *ca.* 0.2 – 0.5 mg/mL) was deposited onto a carbon-coated copper grid, which was pre-treated with absolute ethanol to increase the surface hydrophilicity. After 5 min, the excess of the solution was quickly wicked away by a piece of filter paper. The samples were then negatively stained with 4 μL of 1 wt% phosphotungstic acid (PTA) aqueous solution. After 1 min, the excess PTA solution was quickly wicked away by a piece of filter paper and the samples were left to dry under ambient conditions overnight.

Small angle neutron scattering (SANS) experiments were performed on the 30m instrument (NG-3) at the NIST Center for Neutron Research (NCNR), National Institute of Standards and Technology (NIST). A series of fresh SCK samples was prepared in D_2O for the SANS studies. Each block copolymer as a powder (2 mg) was dissolved in DMF-d_7 (2 mL) and an equal amount of D_2O was added dropwise. Then the solution was dialyzed against D_2O for two days (which brought the volume up to *ca*. 8 mL). The micelle solutions were crosslinked with 2,2′-(ethylenedioxy)bis(ethylamine) (EDDA) crosslinker (dissolved in D_2O) and then the SCK nanoparticle solutions were dialyzed against D_2O. The final concentrations of the SCKs in D_2O were *ca*. 0.25 mg/mL. Samples were loaded in titanium sample cells with 30 mm diameter quartz windows at a 2 mm path distance. Monochromatic neutrons at λ= 6Å and a wavelength spread (Δλ/λ) of 0.14 were incident on the sample. The scattered neutrons were captured by a 64 cm × 64 cm 2D detector. Sample-to-detector distances were applied at 1.33, 4.50, and 13.17 m to cover a large scattering wavevector Q range ($0.004 < Q < 0.4$ Å^{-1}), defined by $Q = (4\pi/\lambda)\sin(\theta/2)$, where λ is the neutron wavelength and θ is the scattering angle. Sample data were corrected for background and empty cell scattering. The scattering length densities (Å^{-1}) used for PAA, PAA and EDDA, PS, and D_2O are $1.39e^{-6}$, $5.82e^{-6}$, $1.41e^{-6}$ and $6.31e^{-6}$, respectively. Intensities were normalized to an absolute scale using main beam transmission measurements and were reduced according to published protocol [50]. The related densities (Table 1) were calculated to compare the differences between the corona of the four samples, and are unitless ratios.

2.3. Synthesis of block copolymers and preparation of nanoparticles

General procedure of preparation of Poly(*tert*-butyl acrylate), P*t*BA, 2 – 3—A flame-dried 100-mL Schlenk flask equipped with a magnetic stir bar was charged with

DDMAT (*S*-dodecyl-*S*′-(α,α′-dimethyl-α″-acetic acid) trithiocarbonate, **1**, 1 eq.), *t*-BA (70 – 200 eq.), azobisisobutyronitrile (AIBN) (0.05 eq.), and 2-butanone (10 – 20 mL). The flask was sealed with a rubber septum and allowed to stir for 10 min at room temperature to ensure homogeneous mixing. The reaction mixture was degassed by several freeze-pump-thaw cycles (> 3), after which the flask was allowed to return to room temperature and was allowed to stir for an additional 10 min. The flask was then immersed into a pre-heated oil bath at 60 °C to start the polymerization. The polymerization was monitored by analyzing aliquots collected at predetermined times by ^{1}H-NMR spectroscopy. As the expected monomer conversion was reached, after *ca*. 3 – 6 h depending on desired block chain lengths, the polymerization was quenched by quick immersion of the reaction flask into liquid N_2 and opening to air. THF (20 mL) was added to the reaction flask and the polymer was purified by precipitation into 2 L of a methanol/ice mixture three times. The precipitants were collected and dried under vacuum overnight to afford **2** and **3** as a yellow powder. IR (KBr): 3000-2900, 1723, 1446, 1366, 1248, 1124, 843, 754 cm^{-1}. ^{1}H NMR ($CDCl_3$): δ 0.85 (t, J = 5 Hz, C***H***$_3$CH$_2$-), 1.19 – 1.90 (br, -CHC***H***$_2$- of the polymer backbone, alkyl chain of initiator, and HOOCC(C***H***$_3$)$_2$-), 1.28 – 1.63 (br, C***H***$_3$C), 2.17 – 2.41 (br, -C***H***CH$_2$- of the polymer backbone), 3.22 – 3.36 (br, -SCSC***H***$_2$-), 4.58 – 4.78 (br, -CH$_2$C***H***S) ppm. ^{13}C NMR ($CDCl_3$): δ 28.1, 32.1 – 37.3, 40.1 – 42.6, 80.4 – 80.6, 172.3 – 174.1 ppm.

P*t*BA$_{52}$, 2—A total of 10.2 g (60% yield, 80% conversion) of the polymer was isolated. M_n^{NMR} = 7100 Da, $M_n^{GPC(RI)}$ = 7500 Da, PDI = 1.07, (T_g) = 50 °C, TGA in N_2: 230–245 °C, 40% mass loss; 245–450 °C, 55% mass loss.

P*t*BA$_{120}$, 3—A total of 12.6 g (70% yield, 67% conversion) of the polymer was isolated. M_n^{NMR} = 15700 Da, $M_n^{GPC(RI)}$ = 16700 Da, PDI = 1.04, (T_g) = 51 °C, TGA in N_2: 230–250 °C, 45% mass loss; 245–450 °C, 50% mass loss.

General procedure for preparation of poly(acrylic acid)-*b*-polystyrene (P*t*BA-*b*-PS) by chain extension of P*t*BA with styrene, 4 – 7—To a flame-dried 50 mL Schlenk flask equipped with a magnetic stir bar, P*t*BA (1 eq.), styrene (200 – 400 eq. based on desired polymer chains), AIBN (0.05 eq.) and 1, 4-dioxane (5 – 10 mL) were added. The flask was sealed with a rubber septum and allowed to stir for 10 min. The reaction mixture was then degassed by several freeze-pump-thaw cycles (>3). After allowing the flask to return to room temperature, it was allowed to stir in a pre-heated oil bath at 60 °C to start the polymerization. The polymerization was monitored by analysis of aliquots taken at various times by ^{1}H NMR spectroscopy. The polymerization was quenched at *ca*. 10 – 70 h (depending on desired block chain lengths) by immersing the flask in liquid nitrogen and opening to air. The reaction mixture was dissolved in THF (5 mL) and precipitated into methanol/water (5:1) mixture twice to yield a fine yellow powdery product, **4** – **7**. The product was collected and dried under vacuum overnight. IR: 3100-2900, 1729, 1447, 1372, 1243, 1148, 849, 829, 760 cm^{-1}. ^{1}H NMR ($CDCl_3$): δ 0.83 (t, J = 5 Hz, C***H***$_3$CH$_2$-), 1.20 – 1.80 (br, –CHC***H***$_2$– of the polymer backbone, alkyl chain of initiator, and HOOCC(C***H***$_3$)$_2$–), 1.30 – 1.61 (br, C***H***$_3$C), 2.18 – 2.27 (br,–C***H***CH$_2$– of the polymer backbone), 3.38 – 3.44 (br, –SCSC***H***$_2$–), 5.22 – 5.68 (br, –CH$_2$C***H***S), 6.65 – 7.21 (br, Ar–***H***) ppm. ^{13}C NMR ($CDCl_3$): δ 28.2, 35.1 – 36.3, 39.5 – 41.6, 80.3, 127.9 – 128.9, 140.3, 170.2 – 173.4 ppm.

P*t*BA$_{52}$-*b*-PS$_{80}$, 4—M_n^{NMR} = 15,500 Da, $M_n^{GPC(RI)}$ = 14,300 Da, PDI = 1.2, $(T_g)_{PtBA}$ = 48 °C, $(T_g)_{PS}$ = 104 °C, TGA in N_2: 225–260 °C, 35% mass loss; 260–450 °C, 50% mass loss. 10% mass remaining above 450 °C. Compound **4** was prepared from **P*t*BA$_{52}$**, **2** (2.0 g, 0.3 mmol). The polymerization was carried out for 10 h before precipitation to afford the final product (0.50 g, 70% yield, 25% conversion).

P*t*BA$_{120}$-*b*-PS$_{100}$, 5—M_n^{NMR} = 26,100 Da, $M_n^{GPC(RI)}$ = 22,500 Da, PDI = 1.1, $(T_g)_{PtBA}$ = 50 °C, $(T_g)_{PS}$ = 106 °C, TGA in N_2: 225–260 °C, 25% mass loss; 260–450 °C, 65% mass loss. 10% mass remaining above 450 °C. Compound **5** was prepared from **P*t*BA$_{120}$**, **3** (1.01 g, 0.064 mmol). The polymerization was carried out for 18 h before precipitation to afford the final product (0.67 g, 80% yield, 50% conversion).

P*t*BA$_{52}$-*b*-PS$_{30}$, 6—M_n^{NMR} = 10,200 Da, $M_n^{GPC(RI)}$ = 8,400 Da, PDI = 1.1, $(T_g)_{PtBA}$ = 48 °C, $(T_g)_{PS}$ = 105 °C, TGA in N_2: 230–255 °C, 30% mass loss; 255–450 °C, 60% mass loss. 10% mass remaining above 450 °C. Compound **6** was prepared from **P*t*BA$_{52}$**, **2** (2.01 g, 0.13 mmol). The polymerization was carried out for 70 h before precipitation to afford the final product (2.5 g, 97% yield, 25% conversion).

P*t*BA$_{120}$-*b*-PS$_{40}$, 7—M_n^{NMR} = 19,900 Da, $M_n^{GPC(RI)}$ = 17,200 Da, PDI = 1.2, $(T_g)_{PtBA}$ = 47 °C, $(T_g)_{PS}$ = 105 °C, TGA in N_2: 225–260 °C, 34% mass loss; 260–450 °C, 56% mass loss. 10% mass remaining above 450 °C. Compound **7** was prepared from **P*t*BA$_{120}$**, **3** (2.5 g, 0.16 mmol). The polymerization was carried out for 15 h before precipitation to afford the final product (0.60 g, 85% yield, 10% conversion).

General procedure of preparation of PAA$_m$-*b*-PS$_n$, 8 – 11—A flame-dried 25 mL round bottom flask equipped with a magnetic stir bar was charged with P*t*BA-*b*-PS **5** (0.50 g – 1.50 g), and 15 mL of dichloromethane. Trifluoroacetic acid (TFA, 10 mL) was added to the stirring solution and the reaction was allowed to stir over night at room temperature, after which the solvent was removed under vacuum. The crude product was resuspended in 10 mL of THF and transferred to a pre-soaked dialysis tubing (MWCO *ca*. 6 – 8 kDa), and dialyzed against nanopure water for 4 days, to remove all of the impurities. The solution was then lyophilized to yield the resulting yellowish solid of PAA$_m$-*b*-PS$_n$, **8** – **11**. IR: 3700-2400, 1710, 1554, 1447, 1410, 1240, 1170, 1061, 1025, 798, 790 cm^{-1}. ^1H NMR ($CDCl_3$): δ 0.85 (t, J = 5 Hz, C***H***$_3$CH$_2$-), 1.36 – 2.46 (br,–CHC***H***$_2$– of the polymer backbone), 3.42 – 3.83 (br, –SCSC***H***$_2$–), 5.65 – 5.87 (br, –CH$_2$C***H***S), 6.65 – 7.21 (br, Ar–***H***) ppm, 11.3 – 13.8 (br, COO***H***). ^{13}C NMR ($CDCl_3$): δ 35.4 – 36.6, 42.5 – 45.6, 127.9 – 128.9, 140.1, 175.2 ppm.

PAA$_{52}$-*b*-PS$_{80}$, 8—M_n^{NMR} = 12,500 Da, $(T_g)_{PAA}$ = 127 °C, $(T_g)_{PS}$ = 106 °C, TGA in N_2: 200–300 °C, 15% mass loss; 300–450 °C, 70% mass loss. 10% mass remaining above 450 °C. **8** was prepared from **P*t*BA$_{120}$-*b*-PS$_{100}$, 4** (0.63 g, 0.040 mmol). A total of 0.58 g of **8** was produced (85% yield).

PAA$_{120}$-*b*-PS$_{100}$, 9—M_n^{NMR} = 19,500 Da, $(T_g)_{PAA}$ = 127 °C, $(T_g)_{PS}$ = 103 °C, TGA in N_2: 200–300 °C, 18% mass loss; 300–450 °C, 72% mass loss. **9** was prepared from **P*t*BA$_{120}$-*b*-PS$_{100}$, 5** (1.51 g, 0.048 mmol). A total of 1.07 g of **9** was produced (95% yield).

PAA$_{52}$-*b*-PS$_{30}$, 10—M_n^{NMR} = 7,400 Da, $(T_g)_{PAA}$ = 130 °C, $(T_g)_{PS}$ = 101 °C, TGA in N_2: 200–290 °C, 17% mass loss; 290–450 °C, 74% mass loss. **10** was prepared from **P*t*BA$_{120}$-*b*-PS$_{100}$, 6** (1.49 g, 0.15 mmol). A total of 0.97 g of **10** was produced (89% yield).

PAA$_{120}$-*b*-PS$_{40}$, 11—M_n^{NMR} = 13,200 Da, $(T_g)_{PAA}$ = 127 °C, $(T_g)_{PS}$ = 99 °C, TGA in N_2: 210–300 °C, 23% mass loss; 300–450 °C, 67% mass loss. **11** was prepared from **P*t*BA$_{120}$-*b*-PS$_{100}$, 7** (0.54 g, 0.025 mmol). A total of 0.44 g of **11** was produced (90% yield).

General procedure for micellization and crosslinking (50% crosslinked) of PAA-*b*-PS to form SCKs, 12 – 15—PAA-*b*-PS (*ca*. 50 mg) polymers were dissolved in DMF (50 mL) in a 250 mL round bottom flask and allowed to stir for 30 min at room

temperature. To this solution, an equal volume of nanopure water was added dropwise *via* a syringe pump over a period of 3 h. The reaction mixture was allowed to stir for additional 24 h at room temperature and dialyzed against nanopure water for 4 days in a presoaked dialysis tubing (MWCO *ca*. 6 – 8 kDa) to afford a micelle solution with a final polymer concentration of *ca.* 0.25 mg/mL. To the micelle solution of PAA_m-*b*-PS_n was added a solution of EDDA in nanopure water (*ca*. 0.007 g/mL, 1.1 eq, nominal 50% crosslinking) dropwise *via* a syringe pump over a period of 2 h. To this solution, 1-[3′-(dimethylamino)propyl]-3-ethyl-carbodiimide methiodide (EDCI) in nanopure water (0.011 g/mL, 1.4 eq) was added dropwise *via* a syringe pump over 20 min and the resulting mixture was allowed to stir overnight before dialysis against nanopure water for 4 days in presoaked dialysis tubing (MWCO.*ca*. 6 – 8 kDa) to afford SCK solutions **12** – **15** with a final polymer concentration of *ca*. 0.25 mg/mL.

SCK of PAA_{52}-*b*-PS_{80}, 12—To a stock solution of PAA_{52}-*b*-PS_{80} aqueous micellar solution (~0.25 mg/mL, 30 mL) prepared from **8** (0.020 g, 1.6 μmol), was added a solution of EDDA in nanopure water (175 μL, 8.3 μmol, 1.1 eq., calculated based on 50% of number of poly(acrylic acid) units). The mixture was allowed to stir for 2 h at room temperature before a solution of EDCI in nanopure water (21 μL, 0.8 μmol, 1.4 eq.) was added. The reaction mixture was stirred for 24 h at room temperature and then transferred to a dialysis tube and dialyzed against nanopure water for 3 days. The resulting SCK solution had a concentration of 0.24 mg/mL.

SCK of PAA_{120}-*b*-PS_{100}, 13—To a stock solution of PAA_{120}-*b*-PS_{100} aqueous micellar solution (~0.25 mg/mL, 30 mL) prepared from **9** (0.02 g, 0.98 μmol), was added a solution of EDDA in nanopure water (256 μL, 0.01 mmol, 1.1 eq., calculated based on 50% of number of poly(acrylic acid) units). The mixture was allowed to stir for 2 h at room temperature before a solution of EDCI in nanopure water (14 μL, 0.5 μmol, 1.4 eq.) was added. The reaction mixture was stirred for 24 h at room temperature and then transferred to a dialysis tube and dialyzed against nanopure water for 3 days. The resulting SCK solution had a concentration of 0.24 mg/mL.

SCK of PAA_{52}-*b*-PS_{30}, 14—To a stock solution of PAA_{52}-*b*-PS_{30} aqueous micellar solution (~0.25 mg/mL, 30 mL) prepared from **10** (0.02 g, 2.6 μmol), was added a solution of EDDA in nanopure water (290 μL, 0.01 mmol, 1.1 eq., calculated based on 50% of number of poly(acrylic acid) units). The mixture was allowed to stir for 2 h at room temperature before a solution of EDCI in nanopure water (36 μL, 1.4 μmol, 1.4 eq.) was added. The reaction mixture was stirred for 24 h at room temperature and then transferred to a dialysis tube and dialyzed against nanopure water for 3 days. The resulting SCK solution had a concentration of 0.25 mg/mL.

SCK of PAA_{120}-*b*-PS_{40}, 15—To a stock solution of PAA_{120}-*b*-PS_{40} aqueous micellar solution (~0.25 mg/mL, 30 mL) prepared from **11** (0.02 mg, 1.5 μmol), was added a solution of EDDA in nanopure water (387 μL, 0.02 mmol, 1.1 eq., calculated based on 50% of number of poly(acrylic acid) units). The mixture was allowed to stir for 2 h at room temperature before a solution of EDCI in nanopure water (21 μL, 0.8 μmol, 1.4 eq.) was added. The reaction mixture was stirred for 24 h at room temperature and then transferred to a dialysis tube and dialyzed against nanopure water for 3 days. The resulting SCK solution had a concentration of 0.25 mg/mL.

2.4. DOX loading and release studies

General procedure for DOX loading experiments into PAA-*b*-PS SCK nanoparticles—To a vial containing a magnetic stir bar and SCK solution (10 mL,

polymer concentration ~ 0.25 mg/mL), a solution of doxorubicin (2.273 mg/mL in DMF and 3 eq of triethylamine, 50 wt% with respect to the SCK) was added. The solution was shielded from light and stirred over night before being transferred to a centrifugal filter device (Amicon Ultra 4, 100 kDa MWCO, Millipore corp., Billerica MA, USA) and washed extensively with 5 mM pH 7.4 PBS at 37 °C to remove free DOX. The filtrate was analyzed by UV-Vis spectroscopy to confirm the removal of free DOX after several washing cycles. The DOX-nanoparticle solution was then reconstituted to a final volume of 5 mL with 5 mM pH 7.4 PBS buffer. The amount of incorporated DOX was determined by UV-Vis spectroscopy (488 nm, $\varepsilon = 13050\ M^{-1}cm^{-1}$ determined by a calibration curve in a 4:1 v/v mixture of DMF and DOX-nanoparticle solution in PBS) [48].

DOX-SCK 16—Prepared from **12**. The final volume of the **DOX-SCK 16** was 9.99 mL with a DOX concentration of 0.27 mg/mL (22 wt%).

DOX-SCK 17—Prepared from **13**. The final volume of the **DOX-SCK 17** was 10.00 mL with a DOX concentration of 0.28 mg/mL (20 wt%).

DOX-SCK 18—Prepared from **14**. The final volume of the **DOX-SCK 18** was 10.01 mL with a DOX concentration of 0.20 mg/mL (16 wt%).

DOX-SCK 19—Prepared from **15**. The final volume of the **DOX-SCK 19** was 10.01 mL with a DOX concentration of 0.22 mg/mL (18 wt%).

General procedure for DOX release experiments—Each DOX-SCK solution was partitioned into two parts of 5 mL each and transferred to a presoaked dialysis cassette (Slide-A-Lyzer, 10 kDa MWCO, Pierce Biotechnology, Rockford IL). The cassette was allowed to stir in a beaker containing 4 L of 5 mM PBS at pH 7.4 and 37 °C for a period of 48 h. Another 5 mL of DOX-nanoparticle solution was also transferred to a presoaked dialysis cassette and allowed to stir in a beaker containing 4 L of 5 mM PBS at pH 5.0 and 37 °C for a period of 60 h. Samples (~1.5 mL) were removed from the cassette at 1, 2, 3, 4, 6, 9, 12, 18, 24, 30, 40, 50, and 60 h, and quickly analyzed by UV-Vis spectroscopy (488 nm) and injected back into the dialysis cassette.

3. Results and discussion

In our previous study [48], we investigated the effects of the core material within SCK nanoparticles (amorphous PS *vs.* semicrystalline P(DA-*co*-ODA)) on the loading and release of DOX. It was found that both of these two classes of SCKs were capable of sequestering sufficient amounts of DOX in the interior of the nanoparticle, due to the favorable ionic and hydrophobic interactions. For the PS core SCKs, a relatively higher loading capacity was observed, which could be attributed to π-π stacking interactions between the aromatic ring moieties of styrene and DOX molecules. In an effort to better understand the parameters governing the loading and release of guest molecules in SCK nanoparticles, we herein present a more comprehensive study on SCKs with retention of the core and shell compositions, PS and PAA, respectively, while varying the overall amphiphilic particle dimensions, including differentiation of the hydrophobic particle core size and hydrophilic, ionic shell thickness, independently.

The dimensions of block copolymer micelles are known to be controlled by the relative and overall volumes occupied by the hydrophilic and hydrophobic polymer chain segments, which are determined by their chain lengths and chemical compositions. A series of SCK nanoparticles was produced from covalent crosslinking of corresponding block copolymer micelles, and therefore, the dimensions of SCKs could be tuned by varying their block

copolymer constituents. Block copolymers were designed to have predominantly hydrophilic or hydrophobic block segments, with sufficient structural differences, to provide measurable changes for the core diameter and/or shell thickness of the resulting nanostructures. These structural discrepancies could further affect the loading and release profiles for molecular cargo.

Four PAA-*b*-PS block copolymers having different relative block lengths and absolute chain lengths were synthesized *via* sequential reversible addition-fragmentation chain transfer (RAFT) polymerization reactions [51–60] of *t*-butyl acrylate (*t*BA) and styrene, followed by removal of the *t*-butyl ester protecting groups (Scheme 1). Beginning from DDMAT, **1**, chain transfer agent, two P*t*BA macro-chain transfer agents (macro-CTAs), with number-averaged degrees of polymerization (DP_n) of 52 (**2**) and 120 (**3**) were prepared by RAFT polymerization of *t*BA. Chain extensions with styrene were then conducted to produce the P*t*BA-*b*-PS block copolymers with different DPs of styrene. In both polymerizations, AIBN was used as the initiator, and a relatively low reaction temperature (~ 60 – 70 °C) was employed to provide sufficient AIBN half-life for controlled polymerization. Complete removal of the *t*-butyl groups of P*t*BA-*b*-PS was achieved by TFA treatment and the structures of the resulting amphiphilic PAA-*b*-PS block copolymers were characterized by IR, ^{1}H NMR and ^{13}C NMR spectroscopies.

The degrees of polymerization and well-defined structures for the polymers were confirmed by a combination of ^{1}H NMR spectroscopy and GPC. GPC analyses of the isolated polymers showed mono-modal molecular weight distributions with polydispersity indices (*PDI*) less than 1.3, indicating the controlled fashion during the polymerization process. Assuming full retention of the trithiocarbonate chain end, ^{1}H-NMR spectra of **2** and **3** allowed for determination of the degrees of polymerization of the *t*BA, by comparing the unique methyl terminus resonating at 0.83 ppm with the broad backbone proton signals from 1.2 to 2.4 ppm, which were in agreement with the GPC data. Maintenance of the trithiocarbonate chain end was further observed during growth of the P*t*BA-*b*-PS block copolymers. In addition, the number average molecular weights determined by GPC for P*t*BA-*b*-PS were in agreement with those calculated by ^{1}H NMR spectroscopy (the PAA-*b*-PS adsorbs onto the column packing material and, therefore, cannot be analyzed directly by GPC). The degrees of polymerization and the number average molecular weights of the P*t*BA-*b*-PS and PAA-*b*-PS block copolymers were calculated based on ^{1}H NMR spectroscopy, by comparing the backbone proton signals to those of the aromatic rings at 6.6 – 7.2 ppm.

The significant differences in composition between the PS and PAA segments were revealed by the thermal properties of these block polymers. Each PAA-*b*-PS block copolymer exhibited two glass transition temperatures, at *ca*. 100 and 127 °C, due to phase segregation of the two block segments in the bulk state. This amphiphilic, phase segregating property was relied upon for self assembly of the block copolymers into discrete nanoscale objects in solution.

The micelles and corresponding SCK nanoparticles were prepared from these four PAA_m-*b*-PS_n amphiphilic block copolymers, by following the conventional aqueous micellization methodology (Figure 1). Water (a selective solvent for the PAA block segment) was introduced to the DMF (a good solvent for both PAA and PS) solutions of block copolymers to form discrete spherical micelles. The PAA shell regions of these micelles were then crosslinked *via* amidation chemistry with 2,2′-(ethylenedioxy)bis(ethylamine) (EDDA), as a diamine crosslinker, in the presence of 1-[3′-(dimethylamino)propyl]-3-ethyl-carbodiimide methiodide (EDCI) to afford SCK nanoparticles (Figure 1). Under the protection of the crosslinked shell layer, the core domain is capable of serving as a nanoscopic host to

encapsulate guest molecules. It was expected that the composition of both the core and shell domains could exert influence on the overall characteristics of the SCK nanoparticles, such as the size, shape, flexibility, loading capacity, and release kinetics and/or extents.

The dimensions of the SCKs (**12–15**), were characterized by TEM (Figure 2) and DLS (Figure 3). The circularly-shaped images observed by TEM suggested that these nanoparticles were spherical with narrow size distributions. The SCKs prepared from the block copolymer precursors with higher PS block length (*i.e.*, DP_{PS} = 80 and 100) formed particles with larger core sizes and aggregation numbers (Table 1). The size effect from larger PAA blocks was not distinguished by TEM, due to the difficulty in measuring accurately the entire particle diameter by the staining methods used in this study. However, the effect of the PAA degree of polymerization on the SCK shell thickness was confirmed by DLS measurements. As the DP_n value of the PAA segments was increased from 52 (**12**) to 120 (**13**), *ca.* 25% increase of the hydrodynamic diameter of the resulting SCKs was observed, with no perceptible variation of the core domain size. For **14** and **15**, a similar trend was also observed. Based upon these data, the volumes occupied by the PS cores and PAA shells, the thicknesses of the PAA shells, and the core-shell interfacial areas were calculated (Table 1). The ratios of the volumes occupied by the PAA shells to those of the PS cores increased from SCK **12–15**, and they correlated directly with the proportions of acrylic acid-to-styrene block lengths for each of the block copolymer precursors. The core-shell interfacial areas per particle for **12** and **13** were larger than for **14** and **15**, but the core-shell interfacial areas for the total number of particles for all samples were approximately equivalent, since there were fewer total particles present in samples **12** and **13**.

SANS data of the SCKs in D_2O solutions were fitted by a smeared polydispersity core-shell sphere (SPCSS) model (Figure 4) [50]. The SPCSS model, which involves a variety of core sizes due to polydispersity and smearing effects, gives the best fitting results. An example of different fitting model comparison for SCK **12** is shown in Figure 4B. For **13** and **14**, scattering intensity increased in the low-Q region, indicating possible aggregation of micelles. However, all of the samples fit well by the SPCSS model to give the results of core sizes and shell thicknesses listed in Table 1. The overall particle dimensions from SANS were similar to the number-average hydrodynamic diameters as determined from DLS. However, the core sizes from SANS fitting were slightly smaller than the particle core diameters observed by TEM, which may be caused by slight distortion of the spherical particles upon adsorption onto the TEM grid. The added EDDA, which went into the corona through condensation with PAA, increased the scattering length density of the corona (from $1.39e^{-6}$ to $5.82e^{-6}$ $Å^{-2}$). Assuming the hydrophobic polystyrene formed a homogeneously-dense core in aqueous solution, the densities of the corona for the four SCK nanoparticles were found to be inversely proportional to the corresponding lengths of the PAA block of the polymer precursors (Table 1) and it was observed that samples with longer PAA block segments had lower coronal densities.

The encapsulation of DOX into SCK nanoparticles was carried out by incubating DOX solutions in DMF with SCKs in aqueous solutions (Figure 5). The organic solvent was used to swell the polystyrene core of the SCKs and provide sufficient DOX concentration to drive the diffusion-controlled loading/encapsulation process. This procedure for loading of DOX into pre-established SCKs was followed so that the dimensions of the SCKs could be accurately controlled and locked-in by the shell crosslinks, without potential complications that can occur for block copolymer assembly in the presence of additives. In addition, if the DOX had been present during the crosslinking reaction employed, carbodiimide-mediated amidation, side reactions between the amine functionality of DOX and the AA residues throughout the micellar shell domain could have occurred, covalently linking the drug to the nanostructure. After 24 h of incubation, the unincorporated DOX molecules were removed

from the DOX-SCK system by centrifugation and extensive washing using a centrifugal-filtration membrane and 5 mM PBS (with 5 mM NaCl) at 37 °C. After the centrifugation/filtration-based washing procedure, each SCK solution was reconstituted to its original concentration by the addition of PBS. The resulting DOX concentrations in the SCKs were calculated from the absorption of DOX at 488 nm. A *ca* 20 wt% loading capacity, relative to the mass of PAA-*b*-PS block copolymer precursors and independent of the SCK composition, was achieved for each SCK. This result indicated that the core size of the SCKs did not affect the overall loading capacity for the entire series of nanoparticle solutions. In fact, even for **14**, with the smallest core volume (700 nm^3), the encapsulated DOX could reach a concentration of ~ 75 μM, which was almost 400 times the SCK nanoparticle concentration. However, on a per particle basis, the larger PS cores gave higher numbers of the DOX molecules per particle. It is well-known that the micellar hydrophobic core domain can sequester DOX through hydrophobic and π-π stacking interactions. Meanwhile, other factors, such as electrostatic interactions and hydrogen bonding between DOX and the functionalities across the micellar shell domain, must also be taken into account for the overall loading capacity of the nanoscale vehicles [38, 62]. Because the ratio of the number of DOX molecules loaded per particle to. the volume of PAA per particle decreased as the volume of PAA per particle relative to volume of PS increased (Table 1), we hypothesize that the DOX preferentially resided at the core-shell interface and/or in the core domain. If the DOX molecules were localized in the shell layer, then these trends would have been increasing in parallel. The PAA shell layer was critical, however, to the diffusion of the DOX, as revealed by release kinetics studies.

The DOX release profiles from the SCK nanoparticles were studied by monitoring the decrease in DOX concentration over time, in dialysis cassettes [63]. Based upon the chemical characteristics of DOX and PAA and similarities with literature studies [62], we hypothesized that the release of DOX from the SCK nanoparticles would be faster and proceed to a greater extent at more acidic pH conditions, compared with the release rate at physiological pH 7.4. Promoted release was considered due to loss of electrostatic interactions between the amine functionality of DOX (pK_a of 8.25 [64]) and the PAA shell regions of the nanoparticles upon protonation of acrylic acid groups at lower pH (pK_a of *ca*. 5) [62]. At pH 7.4, DOX carries a positive charge that can form electrostatic interactions with the negatively-charged deprotonated PAA residues in the shell region of the nanoparticles, whereas at pH 5.0, a majority of the acrylic acid residues would be protonated and the loss of electrostatic interactions would trigger release of DOX. This hypothesis was supported by all four SCK nanoparticles, which exhibited *ca*. 40% release at pH 7.4 and 60% at pH 5.0 over 60 h (Figure 6). In addition, the final extents of release of DOX from the SCKs with smaller cores (**14** and **15**) were lower compared with the SCKs with larger cores (**12** and **13**). These differences could be attributed to more frequent inter-particle exchange of the DOX molecules, enhanced by the higher numbers of **14** and **15** nanoparticles (2–3-fold increase, compared to **12** and **13**, respectively, Table 1). More importantly, however, is the ratios of the volume of PAA to the volume of PS, which increase from SCK **12–15**, in agreement with the relative extents of release, due to the need for the DOX to diffuse through and escape from the PAA shell to be observed as released from the dialysis cassette.

For a quantitative determination of the kinetics of DOX release, the experimental data were fit to an exponential relation for Fickian diffusion of a drug from spherical polymeric devices, the Higuchi equation [65–67]:

$$\frac{M_t}{M_\infty} = kt^{\frac{1}{2}}$$

where M_t/M_∞ is the proportion of drug released at a given time, k is the rate constant of drug release, and t is time. The proportion of DOX release plotted against the square root of release time was approximately linear for the first 50% of drug release (Figure 7), in agreement with the limitations of the Higuchi model. The rate constants, k, calculated from the Higuchi plots, indicated faster release kinetics for the first 50% of drug release at pH 5.0 compared with pH 7.4, for all four SCKs **12** – **15** (Table 2). Faster release at pH 5 indicates that the rate determining step for release involves exit through the shell and not from the core, suggesting that a portion of the DOX resides in the shell and/or at the core-shell interface, in addition to potentially being within the core of the particles.

As control experiments, we studied the release of free DOX from the dialysis cassette, which reached a complete release within 5 h, confirming that the measurements were not complicated by the dialysis cassette. We also found that a complete release of DOX was reached within 30 h from the polymer micelles, with a final extent of release of *ca*. 70% at both pH values (Figure 6 and Table 2). The faster release of DOX from the micelles (k = 0.245 or 0.278 $h^{-½}$ at pH 7.4 or pH 5.0, respectively) compared to the SCKs (k ranges from 0.0431 to 0.136 $h^{-½}$) suggests that crosslinking affects the release, which may be due to a combination of differences in compositions and polymer chain dynamics with the incorporation of crosslinkers.

To further quantitatively understand the differences and similarities in DOX release profiles, model-independent methods, which allow us to calculate f_1, the difference factor, and f_2, the similarity factor, were used (see supplementary data) [68, 69]:

$$f_1 = \frac{\sum_{t=1}^{n} |R_t - T_t|}{\sum_{t}^{n} R_t} \times 100$$

where t is the sampling time, n is the number of samples, R_t is the dissolution value of the reference (measured as the percentage of DOX release for the reference) and T_t is the dissolution value of the sample of interest (measured as the percentage of DOX release from the sample). When the reference profile and the sample profile are identical, f_1 is equal to zero and, generally, the profiles are considered similar with f_1 values up to 15. The f_2 factor is a logarithmic transformation of the sum of squared error of difference between the reference and the sample of interest.

$$f_2 = 50 \times \log\left\{\left[1 + \frac{1}{n}\sum_{t=1}^{n}(R_t - T_t)^2\right]^{-0.5}\right\} \times 100$$

When the reference profile and the sample profile are identical, f_2 is equal to 100 and, generally, the profiles are considered similar when f_2 values are greater than 50.

Both the difference factor f_1 and the similarity factor f_2 revealed that the SCK release profiles were significantly different from the free DOX and micelle release profiles (where all f_1 factors are greater than 15 and all f_2 factors are less than 50). There were similarities between SCK**12** and SCK**13** release profiles (f_1 factors ~ 7 and f_2 factors ~ 70), and SCK**14** and SCK**15** release profiles (f_1 factors ~ 11 and f_2 factors ~ 60). In addition, there are mathematical differences between the release profiles of SCKs with larger cores (SCK**12** and SCK**13**) *vs*. SCKs with smaller cores (SCK**14** and SCK**15**). Moreover, the greatest difference observed for **12** (fastest release) *vs*. **15** (slowest release) is in agreement with the

observation that the ratio of the volume occupied by the PAA shell *vs*. that of the PS core is least for **12** and greatest for **15** (Table 1).

4. Conclusions

In this study, SCK nanoparticles were designed to have various relative and absolute core and shell dimensions to mediate the packaging and release of DOX as a model chemotherapeutic system. Variation over the nanoparticle dimensions was achieved through controlling of the block copolymer precursor chain lengths, to afford a series of well-defined and rigorously characterized nanoscopic vessels for drug molecule loading and release studies. The amphiphilic core-shell morphology of the SCK nanostructures provided opportunities for tuning of the drug loading capacities and rates of release; increasing core diameters and core-shell interfacial surface areas were important for increased guest packaging capacity and decreasing proportions of shell-to-core volume was the critical parameter for increased kinetics of release. The electrostatic complexation of DOX and the PAA shell showed predominant effects on the rates of release, giving accelerated release at acidic pH *vs.* under physiological pH conditions, which may lead to enhanced selectivity of delivery in cancer therapy. Moreover, the amphiphilic core-shell morphology of the SCKs provided opportunities for tuning of the relative contributions of hydrophobic and/or π-π interactions with the core domain and electrostatic interactions with the shell layer to give significant impact on the extents of release of DOX. The variety of contributing factors, of chemical composition, dimensions of the core and shell domains, and total particle concentrations, made direct determination of the effects of each parameter complicated, although the greatest correlation appeared to be the ratio of the volume of the shell *vs*. the volume of the core. As the relative proportion of PAA shell to PS core volumes decreased, the rate and extent of release increased. Because these proportions are conveniently tuned by the nature of the block copolymer precursor, SCK nanoparticles offer enormous opportunity for the production of nanoscopic drug carriers with finely-tuned performance potential. These studies, therefore, point to future directions to craft sophisticated devices for controlled drug release.

Supplementary Material

Refer to Web version on PubMed Central for supplementary material.

Acknowledgments

Financial support from Covidien is gratefully acknowledged. K. L. Wooley serves as a consultant to Covidien. N. S. Lee thanks GlaxoSmithKline for their financial support through the ACS Division of Organic Chemistry Graduate Fellowship. This work was also supported in part by the National Heart Lung and Blood Institute of the National Institutes of Health as a Program of Excellence in Nanotechnology (HHSN268201000046C), by the National Science Foundation (DMR-0906815 and DMR-1032267), and by the Welch Foundation through the W. T. Doherty-Welch Chair in Chemistry, Grant No. A-0001. Assistant Professor fellowship from the Knut and Alice Wallenberg Foundation (to A. M. N), as well as financial support from Åke Wibergs foundation, Karolinska Insitutet, The Swedish Medical Nanoscience Center and from the Swedish Research Council 2009-3259, are also gratefully acknowledged. The authors thank Department of Otolaryngology, Washington University School of Medicine for the access to TEM facility and Center for Neutron Research at National Institute of Standards and Technology for the access to SANS facility.

References

1. Wooley KL. Shell crosslinked polymer assemblies: Nanoscale constructs inspired from biological systems. J Polym Sci Pol Chem. 2000; 38:1397–1407.
2. Kataoka K, Kwon GS, Yokoyama M, Okano T, Sakurai Y. Block-Copolymer Micelles as Vehicles for Drug Delivery. Journal of Controlled Release. 1993:119–132.

3. Cho KJ, Wang X, Nie SM, Chen Z, Shin DM. Therapeutic nanoparticles for drug delivery in cancer. Clinical Cancer Research. 2008; 14:1310–1316. [PubMed: 18316549]
4. Langer R. New Methods of Drug Delivery. Science. 1990; 249:1527–1533. [PubMed: 2218494]
5. Carrico ZM, Romanini DW, Mehl RA, Francis MB. Oxidative coupling of peptides to a virus capsid containing unnatural amino acids. Chemical Communications. 2008:1205–1207. [PubMed: 18309418]
6. Schlick TL, Ding ZB, Kovacs EW, Francis MB. Dual-surface modification of the tobacco mosaic virus. Journal of the American Chemical Society. 2005; 127:3718–3723. [PubMed: 15771505]
7. Hooker JM, Kovacs EW, Francis MB. Interior surface modification of bacteriophage MS2. Journal of the American Chemical Society. 2004; 126:3718–3719. [PubMed: 15038717]
8. Le Droumaguet C, Wang C, Wang Q. Fluorogenic click reaction. Chemical Society Reviews. 2010; 39:1233–1239. [PubMed: 20309483]
9. Li K, Nguyen HG, Lu XB, Wang Q. Viruses and their potential in bioimaging and biosensing applications. Analyst. 2010; 135:21–27. [PubMed: 20024176]
10. Destito G, Yeh R, Rae CS, Finn MG, Manchester M. Folic acid-mediated targeting of cowpea mosaic virus particles to tumor cells. Chemistry & Biology. 2007; 14:1152–1162. [PubMed: 17961827]
11. Koudelka KJ, Destito G, Plummer EM, Trauger SA, Siuzdak G, Manchester M. Endothelial Targeting of Cowpea Mosaic Virus (CPMV) via Surface Vimentin. Plos Pathogens. 2009; 5:10.
12. Strable, E.; Finn, MG. Viruses and Nanotechnology. Springer-Verlag; Berlin, Berlin: 2009. Chemical Modification of Viruses and Virus-Like Particles; p. 1-21.
13. Iha RK, Wooley KL, Nystrom AM, Burke DJ, Kade MJ, Hawker CJ. Applications of Orthogonal "Click" Chemistries in the Synthesis of Functional Soft Materials. Chem Rev. 2009; 109:5620–5686. [PubMed: 19905010]
14. Henselwood F, Liu GJ. Water-soluble nanospheres of poly(2-cinnamoylethyl methacrylate)-block-poly(acrylic acid). Macromolecules. 1997; 30:488–493.
15. Kataoka K, Harada A, Nagasaki Y. Block copolymer micelles for drug delivery: design, characterization and biological significance. Advanced Drug Delivery Reviews. 2001; 47:113–131. [PubMed: 11251249]
16. Freiberg S, Zhu X. Polymer microspheres for controlled drug release. Int J Pharm. 2004; 282:1–18. [PubMed: 15336378]
17. Kabanov AV, Batrakova EV, Alakhov VY. Pluronic((R)) block copolymers for overcoming drug resistance in cancer. Advanced Drug Delivery Reviews. 2002; 54:759–779. [PubMed: 12204601]
18. Kabanov AV, Batrakova EV, Alakhov VY. Pluronic (R) block copolymers as novel polymer therapeutics for drug and gene delivery. Journal of Controlled Release. 2002; 82:189–212. [PubMed: 12175737]
19. Gref R, Minamitake Y, Peracchia MT, Trubetskoy V, Torchilin V, Langer R. Biodegradable long-circulating polymeric nanaspheres. Science. 1994; 263:1600–1603. [PubMed: 8128245]
20. Moghimi SM, Hunter AC, Murray JC. Long-circulating and target-specific nanoparticles: Theory to practice. Pharmacological Reviews. 2001; 53:283–318. [PubMed: 11356986]
21. Lee NS, Li YL, Ruda CM, Wooley KL. Aqueous-only, pH-induced nanoassembly of dual pK(a)-driven contraphilic block copolymers. Chemical Communications. 2008:5339–5341. [PubMed: 18985203]
22. Adams ML, Lavasanifar A, Kwon GS. Amphiphilic block copolymers for drug delivery. Journal of Pharmaceutical Sciences. 2003; 92:1343–1355. [PubMed: 12820139]
23. Lee AS, Gast AP, Butun V, Armes SP. Characterizing the structure of pH dependent polyelectrolyte block copolymer micelles. Macromolecules. 1999; 32:4302–4310.
24. Sumerlin BS, Lowe AB, Thomas DB, McCormick CL. Aqueous solution properties of pH-responsive AB diblock acrylamido copolymers synthesized via aqueous RAFT. Macromolecules. 2003; 36:5982–5987.
25. Engin K, Leeper DB, Cater JR, Thistlethwaite AJ, Tupchong L, McFarlane JD. Extracellular Ph Distribution in Human Tumors. International Journal of Hyperthermia. 1995; 11:211–216. [PubMed: 7790735]

26. Jain R, Shah NH, Malick AW, Rhodes CT. Controlled drug delivery by biodegradable poly(ester) devices: Different preparative approaches. Drug Development and Industrial Pharmacy. 1998; 24:703–727. [PubMed: 9876519]
27. Jain RA. The manufacturing techniques of various drug loaded biodegradable poly(lactide-co-glycolide) (PLGA) devices. Biomaterials. 2000; 21:2475–2490. [PubMed: 11055295]
28. Heller J, Himmelstein KJ. Poly(Ortho Ester) Biodegradable Polymer Systems. Methods in Enzymology. 1985; 112:422–436. [PubMed: 3930918]
29. Gopferich A, Alonso MJ, Langer R. Development and Characterization of Microencapsulated Microspheres. Pharmaceutical Research. 1994; 11:1568–1574. [PubMed: 7870673]
30. Arshady R. Preparation of Biodegradable Microspheres and Microcapsules .2. Polyactides and Related Polyesters. Journal of Controlled Release. 1991; 17:1–21.
31. Zweers MLT, Grijpma DW, Engbers GHM, Feijen J. The preparation of monodisperse biodegradable polyester nanoparticles with a controlled size. Journal of Biomedical Materials Research Part B-Applied Biomaterials. 2003; 66B:559–566.
32. Kalarickal NC, Rimmer S, Sarker P, Leroux JC. Thiol-functionalized poly(ethylene glycol)-b-polyesters: Synthesis and characterization. Macromolecules. 2007; 40:1874–1880.
33. Lele BS, Leroux JC. Synthesis and micellar characterization of novel Amphiphilic A-B-A triblock copolymers of N-(2-hydroxypropyl)methacrylamide or N-vinyl-2-pyrrolidone with poly(is an element of-caprolactone). Macromolecules. 2002; 35:6714–6723.
34. Acharya G, Shin CS, Vedantham K, McDermott M, Rish T, Hansen K, Fu Y, Park K. A study of drug release from homogeneous PLGA microstructures. Journal of Controlled Release. 2010; 146:201–206. [PubMed: 20381555]
35. Khougaz K, Gao ZS, Eisenberg A. Determination of the Critical Micelle, Concentration of Block-Copolymer Micelles by Static Light-Scattering. Macromolecules. 1994; 27:6341–6346.
36. Kabanov AV, Bronich TK, Kabanov VA, Yu K, Eisenberg A. Soluble stoichiometric complexes from poly(N-ethyl-4-vinylpyridinium) cations and poly(ethylene oxide)-block-polymethacrylate anions. Macromolecules. 1996; 29:6797–6802.
37. Astafieva I, Khougaz K, Eisenberg A. Micellization in Block Polyelectrolyte Solutions .2. Fluorescence Study of the Critical Micelle Concentration as a Function of Soluble Block Length and Salt Concentration. Macromolecules. 1995; 28:7127–7134.
38. Choucair A, Soo PL, Eisenberg A. Active loading and tunable release of doxorubicin from block copolymer vesicles. Langmuir. 2005; 21:9308–9313. [PubMed: 16171366]
39. Li, Y.; Sun, G.; Xu, J.; Wooley, KL. Shell Crosslinked Nanoparticles: a Progress Report of their Design for Drug Delivery. In: Peppas, NA.; Hilt, JZ.; Thomas, JB., editors. Nanotechnology in Therapeutics. Horizon Bioscience; Norfolk: 2007. p. 381-407.
40. Thurmond KB, Kowalewski T, Wooley KL. Water-soluble knedel-like structures: The preparation of shell-cross-linked small particles. Journal of the American Chemical Society. 1996; 118:7239–7240.
41. Thurmond KB, Kowalewski T, Wooley KL. Shell cross-linked knedels: A synthetic study of the factors affecting the dimensions and properties of amphiphilic core-shell nanospheres. Journal of the American Chemical Society. 1997; 119:6656–6665.
42. O'Reilly RK, Hawker CJ, Wooley KL. Cross-linked block copolymer micelles: functional nanostructures of great potential and versatility. Chemical Society Reviews. 2006; 35:1068–1083. [PubMed: 17057836]
43. Baugher AH, Goetz JM, McDowell LM, Huang HY, Wooley KL, Schaefer J. Location of fluorotryptophan sequestered in an amphiphilic nanoparticle by rotational-echo double-resonance NMR. Biophysical Journal. 1998; 75:2574–2576. [PubMed: 9788953]
44. Kao HM, Stefanescu AD, Wooley KL, Schaefer J. Location of terminal groups of dendrimers in the solid state by rotational-echo double-resonance NMR. Macromolecules. 2000; 33:6214–6216.
45. Kao HM, O'Connor RD, Mehta AK, Huang HY, Poliks B, Wooley KL, Schaefer J. Location of cholic acid sequestered by core-shell nanoparticles using REDOR NMR. Macromolecules. 2001; 34:544–546.
46. Davis KA, Anseth KS. Controlled Release from Crosslinked Degradable Networks. Critical Reviews in Therapeutic Drug Carrier Systems. 2002; 19:385–423. [PubMed: 12661698]

47. Murthy KS, Ma QG, Clark CG, Remsen EE, Wooley KL. Fundamental design aspects of amphiphilic shell-crosslinked nanoparticles for controlled release applications. Chemical Communications. 2001:773–774.
48. Nystrom AM, Xu ZQ, Xu JQ, Taylor S, Nittis T, Stewart SA, Leonard J, Wooley KL. SCKs as nanoparticle carriers of doxorubicin: investigation of core composition on the loading, release and cytotoxicity profiles. Chemical Communications. 2008:3579–3581. [PubMed: 18654719]
49. Nystrom AM, Wooley KL. Construction of thermoresponsive SCKs through tuning the crystalline melting point of the core domain. Soft Matter. 2008; 4:849–858.
50. Kline SR. Reduction and analysis of SANS and USANS data using IGOR Pro. J Appl Crystallogr. 2006; 39:895–900.
51. Perrier S, Takolpuckdee P. Macromolecular design via reversible addition-fragmentation chain transfer (RAFT)/Xanthates (MADIX) polymerization. Journal of Polymer Science Part a-Polymer Chemistry. 2005; 43:5347–5393.
52. Alidedeoglu AH, York AW, McCormick CL, Morgan SE. Aqueous RAFT polymerization of 2-aminoethyl methacrylate to produce well-defined, primary amine functional homo-copolymers. J Polym Sci Part A: Polym Chem. 2009; 47:5405–5415.
53. Bousquet A, Barner-Kowollik C, Stenzel MH. Synthesis of comb polymers via grafting-onto macromolecules bearing pendant diene groups via the hetero-Diels-Alder-RAFT click concept. J Polym Sci Part A: Polym Chem. 2010; 48:1773–1781.
54. Boyer C, Granville A, Davis TP, Bulmus V. Modification of RAFT polymers via thiol-ene reactions: A general route to functional polymers, new architectures. J Polym Sci Part A: Polym Chem. 2009; 47:3773–3794.
55. Gibson MI, Froehlich E, Klok HA. Postpolymerization modification of poly(pentafluorophenyl methacrylate): Synthesis of a diverse water-soluble polymer library. J Polym Sci Part A: Polym Chem. 2009; 47:4332–4345.
56. Kakwere H, Perrier S. Facile synthesis of star-shaped copolymers via combination of RAFT, ring opening polymerization. J Polym Sci Part A: Polym Chem. 2009; 47:6396–6408.
57. Luzon M, Boyer C, Peinado C, Corrales T, Whittaker M, Tao L, Davis TP. Water-soluble, thermoresponsive, hyperbranched copolymers based on PEG-methacrylates: Synthesis, characterization and LCST behavior. J Polym Sci Part A: Polym Chem. 2010; 48:2783–2792.
58. O'Donnell JM, Kaler EW. Kinetic model of reversible addition-fragmentation chain transfer polymerization in microemulsions. J Polym Sci Part A: Polym Chem. 2010; 48:604–613.
59. Schumers JM, Fustin CA, Can A, Hoogenboom R, Schubert US, Gohy JF. Are o-Nitrobenzyl (Meth)acrylate Monomers Polymerizable by Controlled-Radical Polymerization? Journal of Polymer Science Part A: Polymer Chemistry. 2009; 47:6504–6513.
60. Vo C-D, Rosselgong J, Armes SP, Tirelli N. Stimulus-responsive polymers based on 2-hydroxypropyl acrylate prepared by RAFT polymerization. J Polym Sci Part A: Polym Chem. 2010; 48:2032–2043.
61. Sun G, Hagooly A, Xu J, Nystrom AM, Li ZC, Rossin R, Moore DA, Wooley KL, Welch MJ. Facile, efficient approach to accomplish tunable chemistries and variable biodistributions for shell cross-linked nanoparticles. Biomacromolecules. 2008; 9:1997–2006. [PubMed: 18510359]
62. Tian Y, Bromberg L, Lin SN, Hatton TA, Tam KC. Complexation and release of doxorubicin from its complexes with pluronic P85-b-poly(acrylic acid) block copolymers. Journal of Controlled Release. 2007; 121:137–145. [PubMed: 17630011]
63. Gillies ER, Frechet JMJ. pH-responsive copolymer assemblies for controlled release of doxorubicin. Bioconjugate Chemistry. 2005; 16:361–368. [PubMed: 15769090]
64. Sturgeon RJ, Schulman SG. Electronic absorption-spectra and protolytic equilibria of doxorubicin - direct spectrophotometric determination of microconstants. J Pharm Sci. 1977; 66:958–961. [PubMed: 18593]
65. Brophy MR, Deasy PB. Application of the Higuchi model for drug release from dispersed matrices to particles of general shape. Int J Pharm. 1987; 37:41–47.
66. Higuchi T. Mechanism of sustained-action medication: Theoretical analysis of rate of release of solid drugs dispersed in solid matrices. J Pharm Sci. 1963; 52:1145–1149. [PubMed: 14088963]

67. Serra L, Domenech J, Peppas NA. Drug transport mechanisms and release kinetics from molecularly designed poly(acrylic acid-g-ethylene glycol) hydrogels. Biomaterials. 2006; 27:5440–5451. [PubMed: 16828864]

68. Costa FO, Sousa JJS, Pais A, Formosinho SJ. Comparison of dissolution profiles of Ibuprofen pellets. Journal of Controlled Release. 2003; 89:199–212. [PubMed: 12711444]

69. Moore JW, Flanner HH. Mathematical comparison of dissolution profiles. Pharm Tech. 1996; 20:67–74.

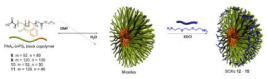

Figure 1.
Schematic representation of the supramolecular assembly of PAA_m-*b*-PS_n block copolymers into micelles and their subsequent crosslinking with EDDA to form SCKs.

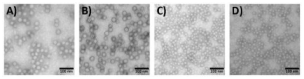

Figure 2.
Characterization of SCKs **12 – 15** by TEM (drop deposited on carbon-coated copper grids and stained negatively with phosphotungstic acid) of A) **12**, B) **13**, C) **14**, and D) **15**.

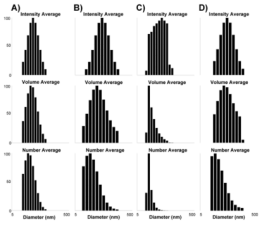

Figure 3.
Characterization of SCKs **12 – 15** by DLS. DLS histograms of intensity-averaged, volume-averaged, number-averaged hydrodynamic diameters: A) SCK **12**, B) SCK **13**, C) SCK **14**, and D) SCK **15** in nanopure water.

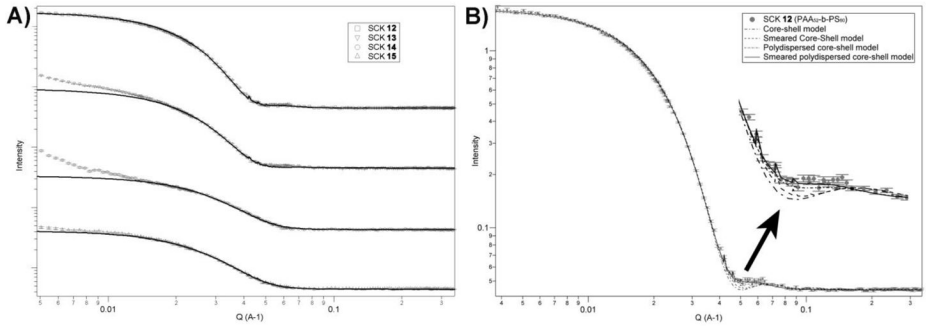

Figure 4.

A). Small angle neutron scattering (SANS) data of SCK **12** – **15**. Black solid lines present fitting curves of “smeared polydispersed core-shell sphere” model. B). Model fitting results for SANS profile of SCK **12** with “core-shell sphere” model, “smeared core-shell sphere” model, “polydispersed core-shell sphere” model and “smeared polydispersed core-shell sphere” model.

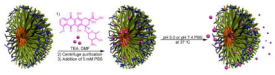

Figure 5.
Schematic representation of the loading of DOX into the core, core-shell interface and shell region of the SCKs while suspended in aqueous solution, and release of DOX from the SCK in pH 5.0 or pH 7.4 buffer at 37 °C.

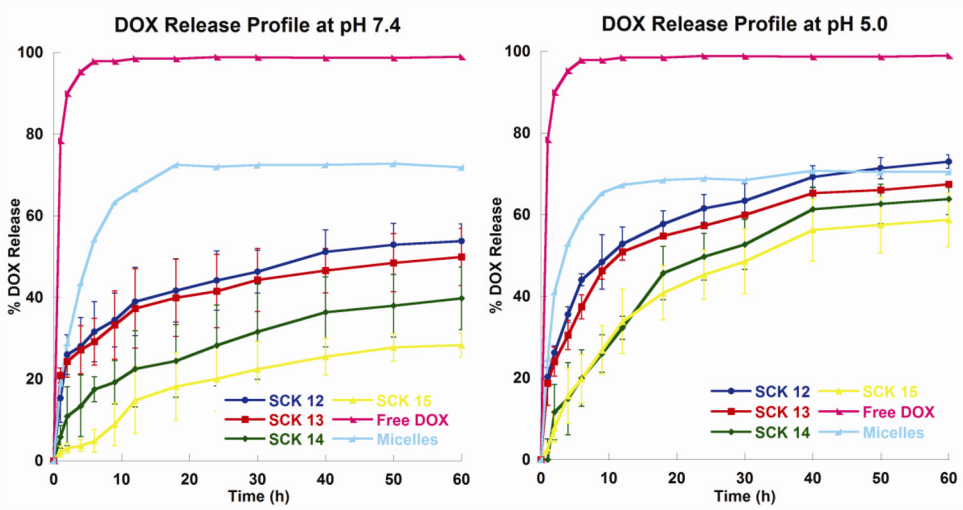

Figure 6.
DOX release profiles of free DOX, micelles, and SCK**12**, SCK**13**, SCK**14** and SCK**15** at pH 7.4 or pH 5.0.

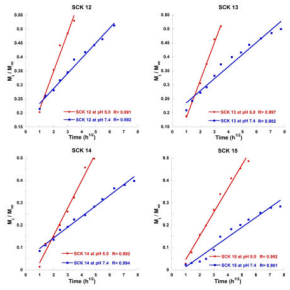

Figure 7.
Higuchi plots of DOX release profiles of SCK**12**, SCK**13**, SCK**14** and SCK**15** at pH 7.4 or pH 5.0.

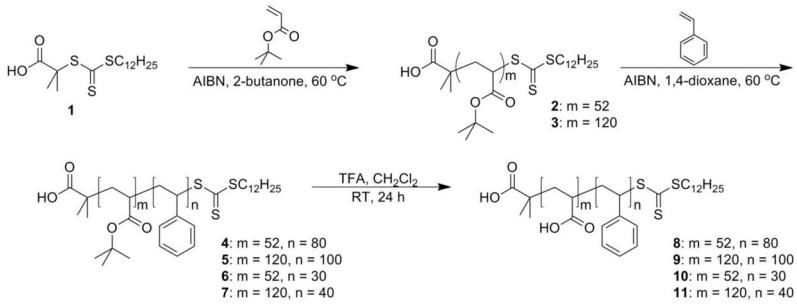

Scheme 1.

Preparation of P*t*BA macro-CTA, chain extension with styrene, and removal of the *tert*-butyl protecting groups to produce PAA_m-*b*-PS_n polymers of various chain lengths.

Table 1

Experimental and calculated dimensions of the SCKs, and quantified DOX loading values.

SCK	**12**	**13**	**14**	**15**
Polymer precursors	**PAA_{52}-*b*-PS_{80}**	**PAA_{120}-*b*-PS_{100}**	**PAA_{52}-*b*-PS_{30}**	**PAA_{120}-*b*-PS_{40}**
D_{TEM} [nm]	19 ± 2	20 ± 2	11 ± 2	13 ± 2
V_{PS} [nm^3]	3600	4200	700	1200
Aggregation number	270	260	140	180
V_{PAA} [nm^3]	1600	3600	830	2500
$T_{shell,\ calc}$ [nm]	1.5	2.3	1.5	3.1
V_{PAA}/V_{PS}	**0.44**	**0.86**	**1.2**	**2.1**
$(D_h)_{Int}$ [nm]	88 ± 6	110 ± 16	81 ± 12	90 ± 12
$(D_h)_{Vol}$ [nm]	30 ± 3	43 ± 6	20 ± 6	35 ± 2
$(D_h)_{Num}$ [nm]	24 ± 2	30 ± 3	14 ± 3	18 ± 3
$SA_{core/particle}$ [nm^2]	1100	1300	380	530
Total # particles [$\times 10^{14}$, 10 mL solution volume]	4.4	3.0	14	6.1
$SA_{core/total}$ [$\times 10^{17}$ nm^2, 10 mL solution volume]	5	4	5	3
$D_{core,SANS}$ [nm]	17.4	15.3	9.0	8.9
Core size polydispersity	0.13	0.11	0.20	0.33
D_{SANS} [nm]	24.4	25.1	17.4	17.3
$T_{shell,\ SANS}$ [nm]	3.5	4.9	4.7	4.2
Related density of shell	4.6	3.0	4.5	2.7
DOX per particle	6400	9700	1500	3800
DOX/V_{PAA}	**4.0**	**2.7**	**1.8**	**1.5**

D_{TEM} = diameter by TEM

V_{ps} = volume of the PS core

Aggregation number calculated based on diameter by TEM using previously reported equation [61]

V_{PAA} = volume of the PAA shell, calculated from the TEM core volume to obtain the block copolymer aggregation number, convert to the PAA mass from the total number of AA repeat units, and finally the volume occupied by PAA was determined using a PAA density of 1.05 g/mL

$T_{shell,\ calc}$ = thickness of the PAA shell in the solid state, estimated from the volume of PAA + volume of PS minus the radius of the PS core

D_h = intensity (Int), volume (Vol), number (Num) average diameters by DLS

$SA_{core/particle}$ = core-shell interfacial area per particle

$SA_{core/total}$ = core-shell interfacial area for total numbers of particles in 10 mL of aqueous solution

$D_{core,SANS}$ = core diameter from SANS

D_{SANS} = particle size from SANS

$T_{shell,\ SANS}$ = shell thickness from SANS

Table 2

DOX release rate, k ($h^{-½}$), obtained from fitting drug release experimental data to the Higuchi model [65–67].

		12	13	14	15	Micelles
		From Polymer Precursors				
		PAA_{52}-*b*-PS_{80}	PAA_{120}-*b*-PS_{100}	PAA_{52}-*b*-PS_{30}	PAA_{120}-*b*-PS_{40}	PAA_{120}-*b*-PS_{40}
pH 7.4	k, $h^{-½}$	0.0540	0.0431	0.0477	0.0441	0.245
pH 5.0	k, $h^{-½}$	0.136	0.134	0.124	0.106	0.278